J Ginseng Res 44 (2020) 50–57

Contents lists available at ScienceDirect

Journal of Ginseng Research

journal homepage: http://www.ginsengres.org

Research Article

Proteomic analyses reveal that ginsenoside Rg3(*S*) partially reverses cellular senescence in human dermal fibroblasts by inducing peroxiredoxin

Ik-Soon Jang [1,☆], Eunbi Jo [1,☆], Soo Jung Park [2,☆], Su Jeong Baek [1], In-Hu Hwang [3], Hyun Mi Kang [4], Je-Ho Lee [1,5], Joseph Kwon [1], Junik Son [6], Ho Jeong Kwon [7,**], Jong-Soon Choi [1,5,*]

[1] *Biological Disaster Analysis Group, Korea Basic Science Institute, Daejeon, Republic of Korea*
[2] *Department of Sasang Constitutional Medicine, College of Korean Medicine, Woosuk University, Wanju, Jeonbuk, Republic of Korea*
[3] *Neuroscience Research Institute, Korea University College of Medicine, Seoul, Republic of Korea*
[4] *Bio & Health Research Institute, ACT (Advanced Cosmeceutical Technology), Suwon, Republic of Korea*
[5] *Graduate School of Analytical Science and Technology, Chungnam National University, Daejeon, Republic of Korea*
[6] *Chung-Ang University College of Medicine, Seoul, Republic of Korea*
[7] *Chemical Genomics Global Research Laboratory, Department of Biotechnology, College of Life Science and Biotechnology, Yonsei University, Seoul, Republic of Korea*

ARTICLE INFO

Article history:
Received 8 January 2018
Received in Revised form
6 July 2018
Accepted 30 July 2018
Available online 13 August 2018

Keywords:
Ginsenoside Rg3(S)
Human dermal fibroblast
Label-free quantitative proteomics
Restoration
Senescence

ABSTRACT

Background: The cellular senescence of primary cultured cells is an irreversible process characterized by growth arrest. Restoration of senescence by ginsenosides has not been explored so far. Rg3(*S*) treatment markedly decreased senescence-associated β-galactosidase activity and intracellular reactive oxygen species levels in senescent human dermal fibroblasts (HDFs). However, the underlying mechanism of this effect of Rg3(*S*) on the senescent HDFs remains unknown.
Methods: We performed a label-free quantitative proteomics to identify the altered proteins in Rg3(*S*)-treated senescent HDFs. Upregulated proteins induced by Rg3(*S*) were validated by real-time polymerase chain reaction and immunoblot analyses.
Results: Finally, 157 human proteins were identified, and variable peroxiredoxin (PRDX) isotypes were highly implicated by network analyses. Among them, the mitochondrial PRDX3 was transcriptionally and translationally increased in response to Rg3(*S*) treatment in senescent HDFs in a time-dependent manner.
Conclusion: Our proteomic approach provides insights into the partial reversing effect of Rg3 on senescent HDFs through induction of antioxidant enzymes, particularly PRDX3.

1. Introduction

Cellular senescence is one of the hallmarks of aging, which is defined as the process of becoming old [1]. During senescence, cells begin to lose their ability to grow and undergo cell division because of the accumulative damage from reactive oxygen species (ROS) that are generated in mitochondria. In response to ROS over a particular threshold, cells pause their cell cycles, which initiates signaling through replicative senescence pathways, such as p16/Rb and p53/p21 [2]. There might be multiple factors that regulate aging; however, the cellular senescence observed in human dermal fibroblasts (HDFs) can be studied to determine possible causes associated with free radical generation stemming from mitochondrial dysfunction. These free radicals exert age-associated aggravation of cellular damage; however, the age-related senescence in cells and tissues can be prevented by intracellular antioxidant systems, such as superoxide dismutase and peroxiredoxins (PRDXs) [3–5]. To mitigate ROS-mediated

* Corresponding author. Biological Disaster Analysis Group, Korea Basic Science Institute, Daejeon, 34133, Republic of Korea.
** Corresponding author. Department of Biotechnology, Yonsei University, Seoul, 03722, Republic of Korea.
E-mail addresses: kwonhj@yonsei.ac.kr (H.J. Kwon), jschoi@kbsi.re.kr (J.-S. Choi).
☆ These authors contributed equally to this work.

https://doi.org/10.1016/j.jgr.2018.07.008
p1226-8453 e2093-4947/$ – see front matter

oxidative damage involved in aging, resveratrol, a polyphenol natural product, was introduced and has been extensively applied to improve health by enhancing cellular redox capability [6].

Likewise, ginseng saponins have been suggested to protect against oxidative damage related to aging in senescent mice, tissues, and human cultured cells [7–9]. Ginseng has been cultivated in North America and eastern Asia—mostly in Korea, northeastern China, Bhutan, and eastern Siberia. Ginseng is a species of perennial plants which belong to the *Panax* genus in the family, *Araliaceae*. *Panax ginseng* (Asian ginseng) and *Panax quinquefolius* (American ginseng) ginsenosides were determined by liquid chromatography–coupled mass spectrometry (MS) for assessing morphology-based variations [10]. Thus, ginseng is known to be an adaptogenic herb. When American ginseng roots are steamed or heated, the ginsenoside profiles are altered, and the content of ginsenosides, Rh2, Rg2, and Rg3(*S*/*R*), is increased. In particular, Rg3, which exhibits strong anticancer activity, was significantly increased [11]. Recently, Rg3-enriched red ginseng extract has been shown to have antiplatelet activity, thus resulting in the alleviation of aging-associated diseases [12]. Rg3 is an effective medicinal compound and can be found as two stereoisomers at C-20: 20(*S*)-Rg3 and 20(*R*)-Rg3. Furthermore, a diglucosyl moiety at the C-3 hydroxyl of Rg3 can be degraded into monoglucosyl Rh2 and aglyconic protopanaxadiol (PPD) by glycoside hydrolases expressed in human intestinal bacteria [13].

It was reported that Rg3 prevents oxidative stress–induced astrocytic senescence and inhibits senescence of prostate stromal cells by modulating inflammatory cytokines [14,15]. In addition to the positive effects on normal cells, Rg3 also promotes senescence and apoptosis of gallbladder cancer cells by activating the p53 pathway [16]. In particular, the Rg3(*S*) and Rg3(*R*) stereoisomers exerted different antiphotoaging effects on UV-B–irradiated keratinocytes [17]. Although many positive effects of Rg3 have been reported, the preventative effects of Rg3(*S*) on HDF cell senescence has not been investigated yet. Herein, senescence-associated β-galactosidase (SA-β-gal) activities and expression levels of senescence marker proteins were compared between HDFs treated with 20(*S*)-stereotypic Rg3, Rh2, aglyconic PPD, and 20(*R*)-stereotypic Rg3. In addition, we performed MS-based proteomics experiments using a label-free shotgun approach to identify proteins whose levels are significantly affected by treatment with Rg3(*S*) in senescent HDFs. The functional ginsenoside proteomics experiments provided several candidate proteins that might be involved in the protective mechanisms associated with Rg3(*S*) treatment of senescent HDFs. These data also suggest that Rg3(*S*) could be a potential therapeutic for treating ROS-induced aging.

2. Materials and methods

2.1. Cell culture and chemicals

Primary HDFs were purchased from the American Type Culture Collection (ATCC) (Manassas, VA, USA). Culturing of HDFs was conducted according to the ATCC protocols. Cells were maintained at 37°C in a humidified atmosphere with 5% CO_2. The ginsenosides Rg3(*S*), Rg3(*R*), Rh2(*S*), and PPD(*S*) for treating cells were purchased from the Ambo Institute (Seoul, Korea). HDF cells were grown to 70-80% confluency, washed three times with phosphate-buffered saline (PBS), and treated with 10 μM ginsenosides for 24 h.

2.2. Cell proliferation assays

HDF cells treated with different concentrations of ginsenoside for 24 h were used to measure cell proliferation with a Cell Counting Kit-8 (Dojindo Laboratories, Kumamoto, Japan) according to the manufacturer's instructions as previously performed [18]. To examine the toxicities of the ginsenosides, young (passage #6) and senescent (passage #17-18) HDF cells were starved in media without fetal bovine serum (FBS) for 4 h before ginsenoside treatment. The concentrations of Rg3(*R*), Rh2(*S*), and PPD(*S*) were fixed at 20 μM, and Rg3(S) was used in the range of 5-160 μM dissolved in culture medium containing 0.1% dimethyl sulfoxide (DMSO), whereas no ginsenoside with the same medium was considered as the control.

2.3. SA-β-gal assays

SA-β-gal activity assay was conducted as previously described [19]. Senescence Cells Histochemical Staining Kit (Sigma-Aldrich, St. Louis, MO, USA) was used to assess senescence in HDFs following the manufacturer's instructions. Test plates were washed twice with PBS, counterstained with Mayers Hematoxylin staining solution (Sigma-Aldrich, St, Louis, MO, USA) for 5 min at room temperature, and washed twice with PBS. HDFs were imaged by phase contrast on a Leica microscope (Leica Microsystems, Rijswijk, the Netherlands) and recorded at a 100× magnification using a digital color camera. Five hundred randomly selected fibroblasts per sample plate were photographed, and the blue-stained fibroblasts were counted and expressed as a percentage of SA-β-gal–stained cells.

2.4. Measurement of ROS

Intracellular ROS levels were measured using the dye 2′,7′-dichlorodihydrofluorescein diacetate (Abcam, Cambridge, MA, USA) as described elsewhere [20]. HDFs were seeded on a 96-well plate and incubated for 24 h. The cells were starved for 4 h and then treated with a ginsenoside that was diluted in PBS at 37°C for 4 h. Cells were then treated with 200 μM hydrogen peroxide (H_2O_2) at 37°C for 2 h, and the dye was added to a final concentration of 20 μM. ROS levels in each sample were measured in triplicate. The absorbed and emitted oxidation products were measured at 485 (excitation) and 538 nm (emission), respectively, on a microplate reader (SpectraMax M4 Microplate Reader; Molecular Devices, Sunnyvale, CA, USA).

2.5. Immunoblot analyses

Total protein was isolated using radioimmunoprecipitation assay buffer consisting of 1% (v/v) NP40, 0.1% (w/v) sodium dodecyl sulfate (SDS), 100 μg/mL phenylmethylsulfonyl fluoride, 0.5% (w/v) sodium deoxycholate, protease inhibitors, and phosphatase inhibitors in PBS. Protein concentrations were determined using a BCA Protein Assay Kit (Thermo Fisher Scientific, USA) Proteins were then separated on 10% SDS-polyacrylamide gels and transferred to polyvinylidene fluoride (PVDF) membranes. Membranes were incubated in 5% skim milk with tris-buffered saline Tween (TBST) at room temperature for 1 h and incubated overnight with primary antibodies. The following proteins were probed with the primary antibodies: p16, p21, p53, phospho-p53, caveolin-1, Hsp60, PRDX1-3, and β-actin (Santa Cruz Biotechnology, Dallas, TX, USA). Membranes were washed with TBST and incubated with horseradish peroxidase–conjugated antibody for 1 h. Protein signals were detected using an ECL Detection Kit (BIOFACT, Daejeon, Korea). The signal intensities for each protein band were quantified using the densitometry program, Image J. v1.48. Statistical analyses were performed using Student *t* test. A p values less than 0.05 were considered statistically significant.

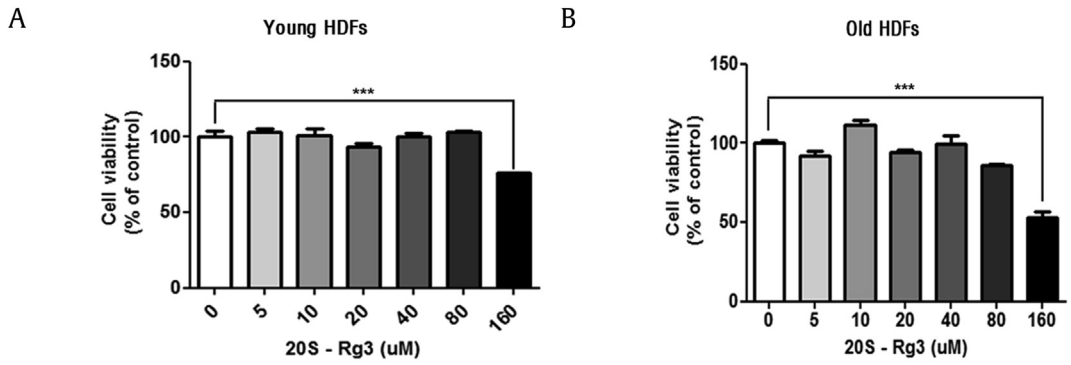

Fig. 1. Cell cytotoxicity of Rg3(*S*) in HDFs. No cytotoxicity was observed in (A) young and (B) old HDFs treated with up to 80 μM of Rg3(*S*). Partial cytotoxicity was observed at 160 μM of Rg3(*S*). HDFs were pretreated with Rg3(*S*) at the given concentration for 24 h at 37°C. Rg3(*S*) was diluted in DMSO (0.1%, v/v), and DMSO alone was used as a control. Cell viability was measured following the CCK-8 protocol.
HDFs, human dermal fibroblasts.

2.6. Tube-gel digestion

A polyacrylamide in-gel digestion of tube gel pieces was performed with slight modification as previously described [21]. In brief, 100 μg of freeze-dried protein was completely solubilized with 6 M urea and denatured at 90°C for 20 min. Proteins were incubated with 10 mM EDTA, 4% SDS, 0.2 M ammonium bicarbonate, and 6 M urea at 37°C for 30 min with intermittent vortexing. The extract was reduced with 200 mM tris (2-carboxyethyl) phosphine hydrochloride and alkylated with 55 mM iodoacetamide at room temperature in the dark for 30 min. The subsequent polymerization, tryptic digestion, and extraction of peptides were same conducted as previously described [21].

2.7. Nano-ultra performance liquid chromatography-MS/MS

The overall procedure was followed by using the previous method with slight modification. Whole protein extracts from HDFs that were treated with Rg3(*S*) for 2, 6, or 12 h were digested as previously described [22]. The peptides were separated using a nanoACQUITY UPLC Chromatography System (Waters Co., Milford, MA; 75 μm × 250 mm, 1.7 μm particle size, BEH300 C_{18} RP analytical column, and a 180 μm × 20 mm Symmetry C_{18} RP 5 μm precolumn). The column temperature was maintained at 30°C. Peptides (5 μL) were injected into the column and eluted with a gradient of mobile phases A and B. Mobile phase A contained 3% acetonitrile and 0.1% formic acid in water, and mobile phase B was composed of 97% acetonitrile and 0.1% formic acid in water. The gradient conditions were as follows: 3% B for 25 min, 3-40% B for 95 min, 40-70% B for 20 min at a flow rate of 300 nL/min and 80% B for 10 min as a rinsing step. For the external calibration, [Glu1]-fibrinopeptide (100 fmol/μL) was delivered as the lock mass compound from the auxiliary pump of the UPLC system at 1 μL/min to the reference sprayer of the NanoLockSpray source in the Synapt' $HDMS^E$ mass spectrometer (Waters Co., Milford, MA).

2.8. Quantitative real-time polymerase chain reaction

Total RNA was extracted from cultured cells with an RNeasy kit (Qiagen, Redwood City, CA, USA). For cDNA synthesis, replicate, quantitative real-time polymerase chain reaction (PCR) was performed with a QuantiTect SYBR Green PCR Kit (Qiagen, Redwood City, CA, USA). All primers were purchased from Bioneer (Daejeon, Korea). The PCR reactions and cycling protocol were performed following the standard protocol provided by Qiagen. Data were collected and analyzed with the $2^{-\Delta\Delta Ct}$ method for quantification to determine relative mRNA expression levels. Oligonucleotide sequences of the primer sets used in this study are listed in Table S1.

2.9. Bioinformatics analyses

Data-independent analysis mode ($LC\text{-}MS^E$) data were processed using PLGS v2.31 (Waters Co., Milford, MA, USA). Peptides were searched against the UniProt database to determine the identities of the proteins (http://www.uniprot.org). The precursor mass tolerance and the fragment tolerance were set to 100 ppm and 0.2 Da, respectively. One missed cleavage with trypsin was allowed during protein identification. Cysteine carbamidomethylation (+57 Da) and methionine oxidation (+16 Da) were chosen as fixed and variable modifications, respectively. The false discovery rates of the peptides identified in PLGS were within 5%. The time-aligned $LC\text{-}MS^E$ precursor ion masses and retention times were within ±10 ppm and ±30 s, respectively. Proteins were considered identified if at least two peptides were assigned to them. The exact mass retention time signature table was constructed using Expression v2 in PLGS to generate the peptide and protein information, including peptide masses and retention times. MS/MS spectra from the data-independent analysis mode were converted into raw files and pkl-files using PLGS software. The combined .pkl files were interpreted using PLGS v2.31 and MASCOT v2.2. For protein network analyses, Ingenuity Pathway Analysis (Ingenuity Systems Inc., Redwood City, CA, USA) was used to predict the functions and pathways associated with the significantly identified proteins. Relative protein expression levels were described as the fold change at a given time point between untreated cells and those treated with Rg3(*S*).

3. Results and discussion

3.1. Rg3(S) restores cellular senescence of HDFs

To determine the optimal concentration of Rg3(*S*) for treating HDFs, we first examined cell viability rates of young and old cells by MTT assays. Cell cytotoxicity of Rg3(*S*) was examined on passage #6 (young) and #17 (old) HDFs using 5-160 μM Rg3(*S*) for 24 h. In both young and old HDFs, no cytotoxicity was observed for concentrations up to 80 μM. However, the high dose of 160 μM Rg3(*S*) decreased the cell viabilities to 25% and 44% in young and old HDFs, respectively (Fig. 1). Contrary to the treatment of 160 μM Rg3(*S*), the treatment of 10 μM Rg3(*S*) in old HDFs showed the highest cell viability. Thus, the concentration of Rg3(*S*) was fixed at 10 μM

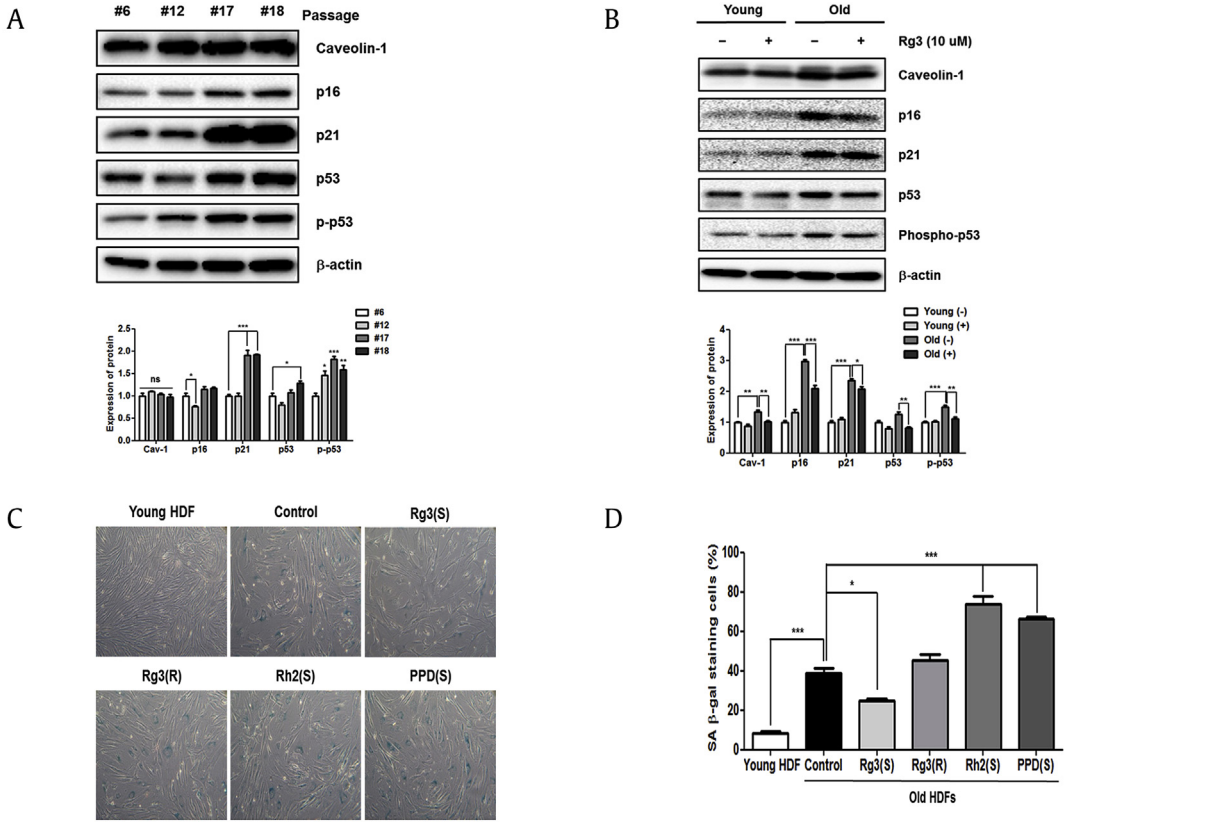

Fig. 2. Immunoblotting of senescence proteins and SA-β-gal staining of Rg3(*S*)-treated senescent HDFs. (A) Immunoblot images of senescence marker expression in successively passaged HDFs. (B) Rg3(*S*)-treated young (passage #6) and old (passage #17) HDFs. HDFs were pretreated with 10 μM Rg3(*S*) for 24 h at 37°C. Rg3(*S*) was diluted in DMSO (0.1%, v/v), and DMSO alone was used as a control. β-Actin was used as a loading control. (C) SA-β-gal staining of senescent HDFs pretreated with Rg3(*S*). (D) Quantification of SA-β-gal staining of Rg3(*S*)-treated old HDFs. Young (passage #6) and old (passage #17) HDFs were incubated with 10 μM of the PPD-type ginsenosides, Rg3(*S*), Rg3(*R*), Rh2(*S*) and PPD(*S*), for 24 h. A representative image of SA-β-gal stained cells is shown. The percentages of SA-β-gal–positive cells were calculated by SABIA (ebiogen, Seoul, Korea) using optical microscopy images. Data represent the mean ± SD of three independent experiments. **Statistical significant of $p < 0.01$.
HDFs, human dermal fibroblasts; PPD, protopanaxadiol; SA-β-gal, senescence-associated β-galactosidase; SD, standard deviation.

Rg3(*S*). Next, to observe the possible replicative senescence, HDF cells derived from ATCC were continuously cultured by changing the culture medium from passage #6 to #18. In general, p16/RB and p53/p21 are considered the classical replicative senescence pathways that are activated in response to external stressors [2]. In addition, senescent cells can undergo caveolin-1–mediated cell cycle arrest through a p53/p21-dependent pathway [23]. The immunoblot analyses revealed increased levels of p16, p21, and p53 in passage #17 and #18 cells (Fig. 2A). Quantification of the relative intensities indicated that the expression level of p21 in passage #17 HDFs was approximately twofold higher than the levels observed in passage #6 HDFs at $p < 0.001$ (Fig. 2A). In addition, the expression levels of p53, and p-p53 in passage #18 cells were increased 1.3-($p < 0.05$) and 1.7-fold ($p < 0.01$), respectively, compared with the levels observed for passage #6 cells. To clarify whether Rg3(*S*) affects HDF cell senescence, the levels of senescence markers were compared between untreated cells and those treated with Rg3(*S*) for both young and old HDFs. The levels of all the senescence proteins, such as caveolin-1, p16, and p53/p21, were decreased at least at $p < 0.01$ in Rg3(*S*)-pretreated old HDFs, whereas the overall expression levels of senescence proteins were not significantly altered in Rg3(*S*)-pretreated young HDFs (Fig. 2B). Quantitation of the immunoblots revealed significant decreases in p16, p21, and p-p53 expression levels in old HDFs treated with Rg3(*S*). This result suggests that Rg3(*S*) partially restores senescence through both p53/p21- and p16-dependent pathways, similar to previous studies showing inhibition of cellular senescence *in vitro* and *in vivo* by Rg1 [24,25].

We examined the possible roles of Rg3(*S*) and other Rg3-derived ginsenosides—Rg3(*R*) (Rg3(*S*) enantiomer), Rh2(*S*) (monoglucosyl form of PPD(*S*)), and PPD(*S*) (aglycone form of Rg3(*S*))—in the senescent HDFs by SA-β-gal staining. Rg3(*S*) exhibited the lowest level of SA-β-gal staining among the tested compounds (Fig. 2C and D). In particular, quantification of SA-β-gal–stained cells revealed that young and old HDFs were 8% and 40% positive for β-galactosidase, respectively. However, cell staining of old HDFs treated with Rg3(*S*) was significantly decreased to 25%, at $p < 0.05$ which is partway between the phenotypes observed for the young and old senescent cells. However, 75% of old HDFs treated with Rh2(*S*) were stained, which was a 1.9-fold increase compared with control old HDFs. Thus, the structure–function relationship of PPD-type ginsenoside restoration against senescence suggests that the diglucosyl moiety at the C-3 hydroxyl and the stereoisomer (*S*) type at C-20 of Rg3 play key roles in restoring partially the senescence process of HDFs. Stereospecific effects of Rg3 were previously reported; Rg3(*R*) was suggested to be a stronger antioxidant and illicit a stronger immune response [26]. In contrast to Rg3(*R*), the 20(*S*) form of Rg3 has a greater solubility, is much less toxic, and has antidiabetic activity [27,28]. These results are in good agreement with the observation that 20(*S*)-Rg3, not 20(*R*)-Rg3, decreased UV-B–induced intracellular ROS levels in keratinocytes [17].

3.2. Specific decrease of ROS production in HDFs by Rg3(S)

As ROS can induce oxidative stress and promote the cellular senescence, we evaluated whether Rg3(*S*) affects the production of

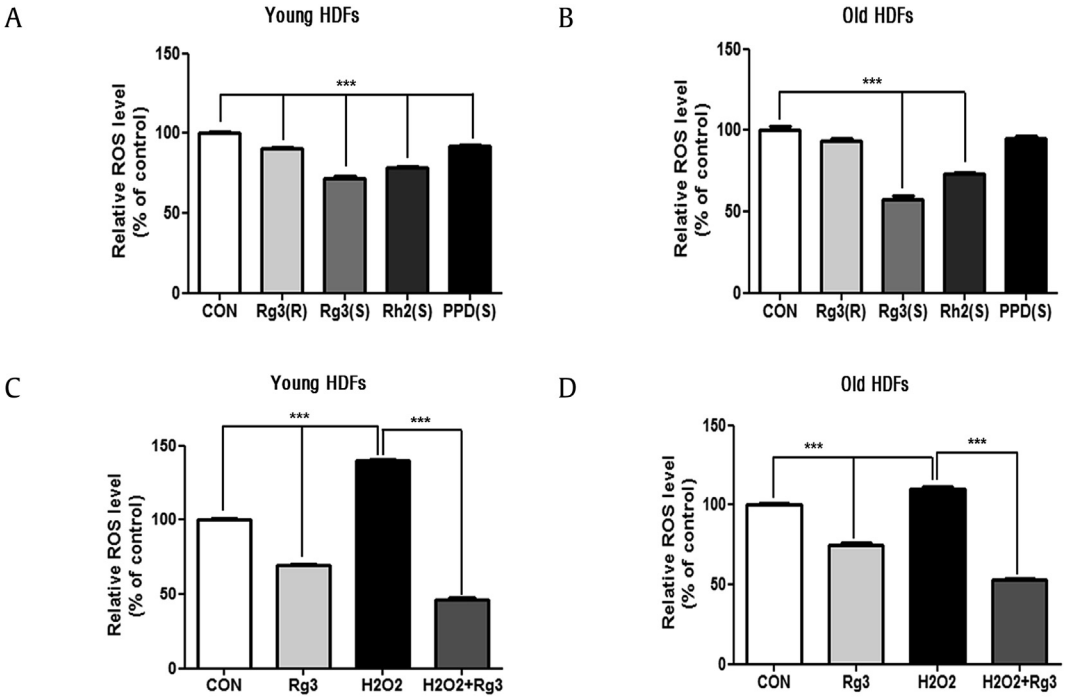

Fig. 3. Native and H_2O_2-induced ROS production in human dermal fibroblasts (HDFs) treated with the indicated PPD-type ginsenosides. (A) Young (passage #6) and (B) old (passage #17) HDFs were pre-incubated with 10 μM of the PPD-type ginsenosides, Rg3(*S*), Rg3(*R*), Rh2(*S*) and PPD(*S*), for 24 h. (C) Young (passage #6) and (D) old (passage #17) HDFs were incubated with 10 μM of Rg3(*S*) for 12 h. Cells were stained with dichlorofluorescein diacetate, fixed, and immediately analyzed using a multianalytic validation system (SpectraMax M4). The data represent the mean ± SD of three independent experiments. **Statistical significant of $p < 0.01$.
H_2O_2, hydrogen peroxide; PPD, protopanaxadiol; ROS, reactive oxygen species; SD, standard deviation.

ROS in HDFs. ROS levels in HDFs were measured by dichlorofluorescein to compare the effects of the PPD-type ginsenosides. Rg3(*S*) significantly decreased intact ROS levels of young and old HDFs by up to 45% and 55% at $p < 0.001$, respectively, compared with the control HDFs (Fig. 3A and B). Rh2(*S*) decreased ROS levels to approximately 30% in both young and old HDFs. However, neither Rg3(*R*) nor PPD(*S*) affected ROS levels. Thus, Rg3(*S*) was the most effective ROS suppressor. These results corroborated our SA-β-gal staining results (Fig. 2C and D). Next, we examined whether Rg3(S) could attenuate H_2O_2-induced ROS production externally by measuring the scavenging activity of Rg3(*S*) in young and old HDFs cotreated with H_2O_2 and Rg3(S). H_2O_2 significantly increased the ROS signal to 40% in young HDFs, whereas the signal was slightly increased to 10% in old HDFs (Fig. 3C and D). Thus, young HDFs appears to be more sensitive to H_2O_2 than old HDFs. Interestingly, co-treatment of Rg3(*S*) and H_2O_2 decreased ROS signal dramatically to 60% and 50% in young and old cells, respectively, compared with singly H_2O_2-treated cells. These data suggest that Rg3(*S*) lowers ROS levels and could be a possible therapeutic for treating oxidative stress-induced senescence. These results closely agree with a previous report suggesting that the ginsenosides, Rh2 and Rg3, inhibit cell proliferation and induce cell apoptosis by increasing mitochondrial ROS levels in human leukemia Jurkat cells [29]. Thus, the decreased SA-β-gal staining and ROS levels by Rg3(*S*) are consistent with the conclusion that Rg3(*S*) attenuates H_2O_2-induced ROS production in HDFs in a stereo-specific manner. Recently, the attenuation of H_2O_2-mediated oxidative stress by treatment with Rg3 was reported for HepG2 human hepatocarcinoma cells and in an *in vitro* sepsis model [30,31].

3.3. Proteomic alteration of old HDFs by Rg3(S)

To investigate protein expression levels during an Rg3(*S*)-treatment time course, senescent HDFs were analyzed by nano-UPLC-QTOF tandem MS using data-independent MS^E technology as previously described [32]. Of the original 1327 peptides and 599 proteins observed in the first identification step, 157 human proteins were identified from assignment of two more peptides among the triplicate experiments. The average ratios of 2-h, 6-h, and 12-h treatment of Rg3(*S*) versus the untreated group were 1.1-, 2.3-, and 1.8-fold, respectively. Thus, the 6-h treatment of Rg3(*S*) in senescent HDFs revealed the most dramatic differences in the expression of individual proteins. A list of the identified whole proteins is presented in Table S1. Significantly different levels of proteins at *p*-value < 0.05 were identified: 78 (2 h vs. 0 h), 100 (6 h vs. 0 h), and 60 (12 h vs. 0 h). After 6 h of Rg3(*S*) treatment, 40 significantly upregulated and 16 significantly downregulated proteins with more than a 1.5-fold difference in level were identified. The whole proteins that were different at each time point were subjected to protein network analyses using Ingenuity Pathway Analysis. The main subnetwork 1 containing PRDX3 belonged to subnetwork 7 was displayed in a time-course pattern of Rg3(*S*) treatment (Fig. 4). As shown in the protein networks, keratin cluster proteins (Krt-1, -2, -4, -5, -6B, -9, -10, -13, -15, -33B) within subnetwork 1 appeared to fluctuate in expression but were mostly downregulated at 6 h of Rg3(*S*) treatment. These findings are in good agreement with a previous study suggesting that the ginsenoside, F2, downregulates keratins, such as Krt2, Krt10, Krt16, in human gastric carcinoma cells [33]. It was suggested that *de novo* synthesis of Rg3(*S*)-responsive regulatory proteins was triggered and caused the downregulation of structural proteins, such as keratins, in senescent HDFs.

The relative abundancies of Rg3(*S*)-induced core proteins with significantly different expressions are listed in Table 1. PPP2R1A (serine/threonine protein phosphatase 2A) levels were the most affected by Rg3(*S*), which was increased by 2.7-, 26.3-, and 11.9-fold at 2, 6, and 12 h, respectively. PPP2R1A interacts with VIM, CAPN2, and EIF4A1 and is also suggested to connect with the core of the NF-κB complex. Upregulation of PPP2R1A by Rg3(*S*) was consistent

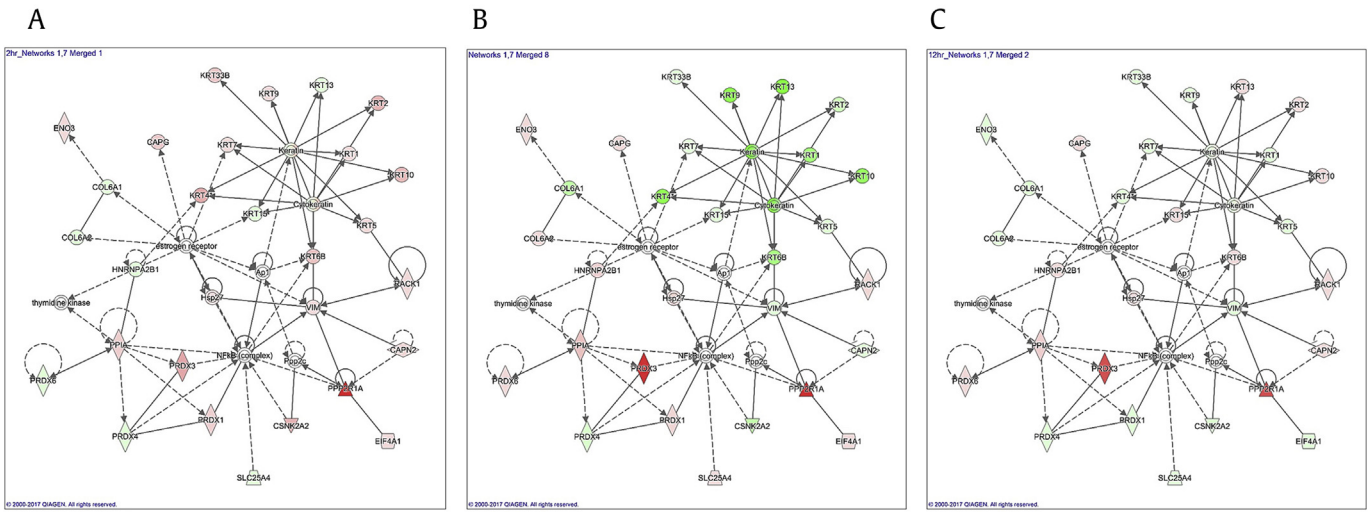

Fig. 4. Protein networks of Rg3(*S*)-treated senescent human dermal fibroblasts (HDFs). The directly interacting networks of proteins from old HDFs treated with 10 μM of Rg3(*S*) for (A) 2 h, (B) 6 h, and (C) 12 h were determined by Ingenuity Pathway Analysis. At each time point, networks 1 (main subnetwork) and 7 (peroxyredoxin-3—containing subnetwork) were merged to determine the molecular functional group. Red and green symbols indicate the proteins that are upregulated and downregulated, respectively, after Rg3(*S*) treatment.

with the previous observation that protein phosphatase A2 inactivation promotes the accumulation of NF-κB—dependent oxidative stress and upregulation of inflammatory processes during aging [34]. We focused on the marginal network proteins containing PRDX isotypes and PPIA (peptidyl-prolyl *cis-trans* isomerase A) because the mitochondrial peroxiredoxin, PRDX3, was dramatically increased by 26.3-fold and PPIA was increased by 2.3-fold after 6 h of treatment with Rg3(*S*). Interestingly, our finding is quite consistent with a previous report suggesting that downregulation of PRDX3 induces cellular senescence of human trophoblasts [35]. Thus, it is notable that Rg3(*S*) can induce expression of ROS-scavenging antioxidant enzymes in mitochondria to prevent the progression of senescence in old HDFs.

3.4. Validation of aging-related proteins in HDF cells treated with Rg3(S)

From the label-free, comparative proteomic analyses, PRDXs, such as PRDX1, PRDX3, PRDX4, and PRDX6, were identified throughout 2—12 h treatment of Rg3(*S*) in senescent HDFs. The expression level of mitochondrial PRDX3 was dramatically increased by 22.5-fold after 6 h of treatment with Rg3(*S*), whereas that of the other PRDXs only fluctuated or were slightly downregulated (Table S1). As the protein network in Fig. 4 shows, cytosolic PRDX1 was a highly abundant antioxidant enzyme, which can interact with the secretory form of PRDX4 [36]. PRDX3 is located in the mitochondrial matrix where it regulates H_2O_2 levels and subsequent signaling processes [37]. PRDXs are ROS-scavenging antioxidant enzymes that are considered to protect against aging. However, few proteomic analyses of the effect of mitochondrial-type PRDX3 on aging in HDFs have been studied.

To validate the Rg3(*S*)-dependent alterations in PRDX isoform and PPIA levels identified by the proteomic analyses, quantitative real-time PCR was performed using a gene-specific primer set. Overall, mRNA expression patterns were similar to those observed in the proteomic analyses, except for PRDX4 (Table S3). PRDX1 and PRDX3 manifested very similar expression patterns, and the changes were statistically significant. These discrepancies between mRNA levels and protein abundances can be attributed to different transcriptional and translational regulations [38]. The abundances

Table 1
Relative abundance of core proteins with the significantly differential protein expression in Rg3(S)-pretreated senescent HDFs

Protein name	Symbol	UnitProt	Peptide count	Ratio[a]			*p* Value[b]		
				2 h/0 h	6 h/0 h	12 h/0 h	2 h/0 h	6 h/0 h	12 h/0 h
Serine/threonine protein phosphatase 2A	PPP2R1A	P30153	2	+5.73	+26.25	+11.9	0.15	0.00	0.06
Peroxiredoxin-3, mitochondrial	PRDX3	P30048	3	+1.88	+22.52	+11.59	0.59	0.02	0.10
Peptidyl-prolyl cis-trans isomerase A	PPIA	P62937	5	+1.41	+2.26	+1.83	0.09	0.00	0.01
Heat shock protein β-1 (Hsp27)	HSPB1	P04792	4	+1.02	+1.85	+1.55	0.72	0.00	0.00
Heterogeneous nuclear ribonucleoproteins A2/B1	HNRNPA2B1	P22626	6	−1.10	+1.82	+1.45	0.61	0.00	0.38
Peroxiredoxin-1	PRDX1	Q06830	6	+1.38	+1.71	−1.06	0.12	0.01	0.88
Receptor of activated protein C kinase 1	RACK1	P63244	6	+1.13	+1.69	+1.26	0.05	0.01	0.18
Peroxiredoxin-6	PRDX6	P30041	7	−1.16	+1.63	+1.33	0.05	0.03	0.11
Casein kinase II subunit α′	CSNK2A2	P19784	5	+1.73	−1.69	−1.75	0.00	0.00	0.04
Collagen α-1(VI) chain	COL6A1	P12109	11	−2.33	−1.75	−1.72	0.00	0.00	0.01
Keratin type II, cytoskeletal 6B	KRT6B	P48669	10	+1.55	−2.27	+1.04	0.01	0.00	0.40
Keratin type II, cytoskeletal 1	KRT1	P04264	33	+1.20	−2.38	+1.04	0.01	0.00	0.40
Keratin type I, cytoskeletal 10	KRT10	P13645	29	+1.64	−2.94	+1.05	0.00	0.00	0.57
Keratin type II, cytoskeletal 4	KRT4	P19013	6	+1.10	−3.33	−1.37	0.30	0.00	0.00
Keratin type I, cytoskeletal 9	KRT9	P35527	19	+1.26	−3.33	−1.33	0.02	0.00	0.30
Keratin type I, cytoskeletal 13	KRT13	P13646	5	−1.03	−3.70	+1.03	0.90	0.00	0.93

[a] Ratio measured by MSE methods. Sign (+) and (−) represent the fold change of upregulation and downregulation, respectively.
[b] *P*-value calculated from individual peak intensities from all tryptic peptides detected per protein.

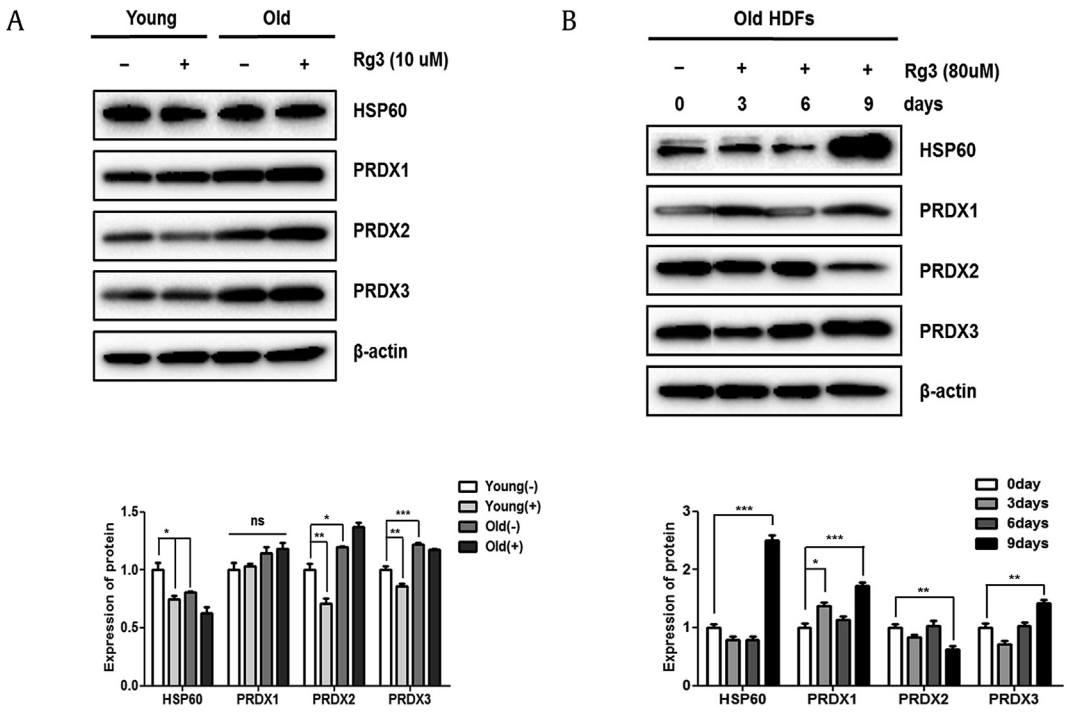

Fig. 5. Immunoblotting of Rg3(*S*)-induced proteins in human dermal fibroblasts (HDFs). (A) Young (passage #6) and old (passage #17) HDFs were pretreated with 10 μM Rg3(*S*) for 24 h. (B) Old HDFs were incubated with a high dose of Rg3(*S*) (80 μM) for 3 to 9 days. At each time point, cells were collected, and the expression levels of Hsp60, PRDX, PRDX2, and PRDX3 were analyzed by immunoblotting. To compare relative expression levels, β-actin was used as loading control. Quantification of protein expression levels was performed using ImageJ. Statistical significance: $^{*}p < 0.05$, $^{**}p < 0.01$, $^{***}p < 0.001$.
PRDX, peroxiredoxin.

of PRDX isoforms were measured by immunoblotting whole cell lysates of senescent HDFs treated with Rg3(*S*) between 24 h and 9 days. As shown in Fig. 5A, differences in expression levels of PRDXs between young and old HDFs were observed only for PRDX2 and PRDX3. In particular, the protein expression levels of PRDX3 in HDFs treated with 80 μM Rg3(*S*) for 9 days increased by 40%, as shown in Fig. 5B. The expression levels of PRDX1 also increased by 80% in that the same condition, but the overall abundance of PRDX1 was lower than that of PRDX3. PRDX2—the supplementary form—decreased after 9 days of treatment with 80 μM Rg3(*S*). Therefore, it seems to be regulated differently by Rg3(*S*) during the cellular senescence of HDFs. No differences were observed in Hsp60 abundance but were observed between untreated senescent HDFs and those treated with Rg3(*S*). However, when HDFs were treated with the cell-tolerant concentration of 80 μM Rg3(*S*) for 9 days, a dramatic increase in Hsp60 level was observed. This result is similar to previous studies that showed mitochondrial Hsp60 increased with age in mollusks and serum Hsp60 increased in aged individuals [39,40]. It is notable that oxidative stress induced a decrease in mitochondrial Hsp60 levels and a concomitant increase in cytosolic Hsp60 in young HDFs but not in old cells [41]. It remains to be clarified the possible translocation of Hsp60 and the protective mechanism of Rg3(*S*) in senescent HDFs later. We have also observed that *Caenorhabditis elegans* that fed on Rg3(*S*) had longer life spans (data not shown). Similarly, there were several reports that suggested PRDXs are involved in life span extension. Knockout mice with PRDX1 showed shortened life spans, and PRDX2 silencing decreased the life span of *C. elegans* [42,43]. In addition, protein levels of mitochondrial PRDX3 were shown to be reduced during aging process [44]. Thus, Rg3(*S*) appears to induce mitochondrial PRDX expression to prevent further aging in HDFs and partly restores their functions to those observed in younger HDFs. Taken together, PRDX3 could be a key player in Rg3(*S*)-induced partial restoration of cellular senescence in HDFs. This systematic study of ginsenoside biochemistry combined with functional proteomics will provide valuable insights into understanding senescence with respect to prevention and the possible therapeutic application of ginseng saponins.

Conflicts of interest

All authors have no conflicts of interest to declare.

Acknowledgements

The present study was supported by the Korea Basic Science Institute research grant (C39712) awarded to J.S. Choi and 2017R1D1A1B03034936. Also, this work was supported by Innopolis Foundation through Technology Commercialization services, funded by Ministry of Science and ICT (2019JBRD0004) to I.S. Jang. This work was partly supported by the Korean Government (MEST; 2015K1A1A2028365, 2015M3A9C 4076321) through the Brain Korea 21 Plus Project, Republic of Korea, which was awarded to H.J. Kwon.

Appendix A. Supplementary data

Supplementary data related to this article can be found at https://doi.org/10.1016/j.jgr.2018.07.008.

References

[1] Lopez-Otin C, Blasco MA, Partridge L, Serrano M, Kroemer G. The hallmarks of aging. Cell 2013;153:1194–217.
[2] Salama R, Sadaie M, Hoare M, Narita M. Cellular senescence and its effector programs. Genes Dev 2014;28:99–114.

[3] Watanabe K, Shibuya S, Koyama H, Ozawa Y, Toda T, Yokote K, Shimizu T. Sod1 loss induces intrinsic superoxide accumulation leading to p53-mediated growth arrest and apoptosis. Int J Mol Sci 2013;14:10998–1010.
[4] Neumann CA, Krause DS, Carman CV, Das S, Dubey DP, Abraham JL, Bronson RT, Fujiwara Y, Orkin SH, Van Etten RA. Essential role for the peroxiredoxin Prdx1 in erythrocyte antioxidant defense and tumour suppression. Nature 2003;424:561–5.
[5] Han YH, Kim HS, Kim JM, Kim SK, Yu DY, Moon EY. Inhibitory role of peroxiredoxin II (Prdx II) on cellular senescence. FEBS Lett 2005;579:4897–902.
[6] Pandey KB, Rizvi SI. Resveratrol up-regulates the erythrocyte plasma membrane redox system and mitigates oxidation-induced alterations in erythrocytes during aging in humans. Rejuvenation Res 2013;16:232–40.
[7] Yokozawa T, Satoh A, Cho EJ. Ginsenoside-Rd attenuates oxidative damage related to aging in senescence-accelerated mice. J Pharm Pharmacol 2004;56:107–13.
[8] Zhao HF, Li Q, Li Y. Long-term ginsenoside administration prevents memory loss in aged female C57BL/6J mice by modulating the redox status and up-regulating the plasticity-related proteins in hippocampus. Neuroscience 2011;183:189–202.
[9] Oh SJ, Oh Y, Rhu IW, Kim K, Lim CJ. Protective properties of ginsenoside Rb3 against UV-B radiation-induced oxidative stress in HaCaT keratinocytes. Biosci Biotechnol Biochem 2015;80:95–103.
[10] Chen Y, Zhao Z, Chen H, Brand E, Yi T, Qin M, Liang Z. Determination of ginsenosides in Asian and American ginsengs by liquid chromatography-quadrupole/time-of-flight MS: assessing variations based on morphological characteristics. J Ginseng Res 2017;41:10–22.
[11] Wang CZ, Aung HH, Zhang B, Sun S, Li XL, He H, Xie JT, He TC, Du W, Yuan CS. Chemopreventive effects of heat-processed *Panax quinquefolius* root on human breast cancer cells. Anticancer Res 2008;28:2545–51.
[12] Jeong D, Irfan M, Kim SD, Kim S, Oh JH, Park CK, Kim HK, Rhee MH. Ginsenoside Rg3-enriched Red Ginseng Extract Inhibits Platelet Activation and *in vivo* thrombus formation. J Ginseng Res 2017;41:548–55.
[13] Zhang H, Li Z, Zhou Z, Yang H, Zhong Z, Lou C. Antidepressant-like effects of ginsenosides: a comparison of ginsenoside Rb3 and its four deglycosylated derivatives, Rg3, Rh2, compound K, and 20-protopanaxadiol in mice models of despair. Pharmacol Biochem Behav 2016;140:17–26.
[14] Hou J, Kim S, Sung C, Choi C. Ginsenoside Rg3 prevents oxidative stress-induced astrocytic senescence and ameliorates senescence paracrine effects on glioblastoma. Molecules 2017;22:E1516.
[15] Peng Y, Zhang R, Kong L, Shen Y, Xu D, Zheng F, Liu J, Wu Q, Jia B, Zhang J. Ginsenoside Rg3 inhibits the senescence of prostate stromal cells through down-regulation of interleukin 8 expression. Oncotarget 2017;8:64779–92.
[16] Zhang F, Li M, Wu X, Hu Y, Cao Y, Wang X, Xiang S, Li H, Jiang L, Tan Z, et al. 20(S)-ginsenoside Rg3 promotes senescence and apoptosis in gallbladder cancer cells via the p53 pathway. Drug Des Devel Ther 2015;9:3969–87.
[17] Lim CJ, Choi WY, Jung HJ. Stereoselective skin anti-photoaging propertied of ginsenoside Rg3 in UV-B-irradiated keratinocytes. Biol Pharm Bull 2014;37:1583–90.
[18] Sohn EJ, Kim JM, Kang SH, Kwon J, An HJ, Sung JS, Cho KA, Jang IS, Choi JS. Restoring effects of natural anti-oxidant quercetin on cellular senescent human dermal fibroblasts. Am J Chin Med 2018;46:853–73.
[19] Dimri GP, Lee X, Basile G, Acosta M, Scott G, Roskelley C, Medrano EE, Linskens M, Rubelj I, Pereira-Smith O, et al. A biomarker that identified senescent human cells in culture and in aging skin in vivo. Proc Natl Acad Sci USA 1995;92:9363–7.
[20] Eruslanov E, Kusmartsev S. Identification of ROS using oxidized DCFDA and flow-cytometry. Meth Mol Biol 2010;594:57–72.
[21] Yu H, Wakim B, Li M, Halligan B, Tint GS, Patel SB. Quantifying rat proteins in neonatal mouse brain by 'tube-gel' protein digestion label-free shotgun proteomics. Proteome Sci 2007;5:17.
[22] Kwon J, Park SH, Park C, Kwon SO, Choi JS. Analysis of membrane proteome by data-dependent LC-MS/MS combined with data-independent LC-MSE technique. J Anal Sci Tech 2010;1:78–85.
[23] Galbiati F, Volonte D, Liu J, Capozza F, Frank PG, Zhu I, Pestell RG, Lisanti MP. Caveolin-1 expression negatively regulates cell cycle progression by inducing G_0/G_1 arrest via a p53/$p21^{WAF1/Cip1}$-dependent mechanism. Mol Biol Cell 2001;12:2229–44.
[24] Li SG, Yan MZ, Zhang D, Ye M, Deng JJ. Effects of ginsenoside Rg1 on the senescence of vascular smooth muscle cells. Genet Mol Res 2016;15:15038409.
[25] Chen C, Mu XY, Zhou Y, Shun K, Geng S, Liu J, Wang JW, Chen J, Li TY, Wang YP. Ginsenoside Rg1 enhances the resistance of hematopoietic stem/progenitor cells to radiation-induced aging in mice. Acta Pharmacol Sin 2014;35:143–50.
[26] Wei X, Su F, Su X, Hu T, Hu S. Stereospecific antioxidant effects of ginsenoside Rg3 on oxidative stress induced by cyclophosphamide in mice. Fitoterapia 2012;83:636–42.
[27] Park MW, Ha J, Chung SH. 20(S)-ginsenoside Rg3 enhances glucose-stimulated insulin secretion and activates AMPK. Biol Pharm Bull 2008;31:748–51.
[28] Liu JP, Lu D, Nicholson RC, Zao WJ, Li PY, Wang F. Toxicity of a novel anti-tumor agent 20(S)-ginsenoside Rg3 via CHOP-mediated DR5 upregulation in human hepatocellular carcinoma cells. Mol Cancer Ther 2012;12:274–85.
[29] Xia T, Wang YN, Zhou CX, Wu LM, Liu Y, Zeng QH, Zhang XL, Yao JH, Wang M, Fang JP. Ginsenoside Rh2 and Rg3 inhibit cell proliferation and induce apoptosis by increasing mitochondrial reactive oxygen species in human leukemia Jurkat cells. Mol Med Rep 2017;15:3591–8.
[30] Bak MJ, Jeong WS, Kim KB. Detoxifying effect of fermented black ginseng on H_2O_2-induced oxidative stress in HepG2 cells. Int J Mol Med 2014;34:1516–22.
[31] Xing W, Yang L, Peng Y, Wang Q, Gao M, Yang M, Xiao X. Ginsenoside Rg3 attenuates sepsis-induced injury and mitochondrial dysfunction in liver via AMPL-mediated autophagy flux. Biosci Rep 2017;39:20170934.
[32] Moon YJ, Kwon J, Yun SH, Lim HL, Kim MS, Kang SG, Lee JH, Choi JS, Kim SI, Chung YH. Proteome analyses of hydrogen-producing hyperthermophilic archaeon *Thermococcus onnurineus* NA1 in different one-carbon substrate culture conditions. Mol Cell Proteomics 2012;11:M111. 015420.
[33] Mao Q, Zhang PH, Yang J, Xu JD, Kong M, Shen H, Zhu H, Bai M, Zhou L, Li GF, et al. iTRAQ-based proteomic analysis of ginsenoside F2 on human gastric carcinoma cells SGC7901. Evidence Based Comp Altern Med 2016:2635483.
[34] Jung KJ, Kim DH, Lee EK, Song CW, Yu BP, Chung HY. Oxidative stress induces inactivation of protein phosphatase 2A, promoting proinflammatory NF-κB in aged rat kidney. Free Rad Biol Med 2013;61:206–17.
[35] Wu WB, Menon R, Xu YY, Zhao JR, Wang YL, Liu Y, Zhang HJ. Down-regulation of peroxiredoxin-3 by hydrophobic bile acid induces mitochondrial dysfunction and cellular senescence in human trophoblasts. Sci Rep 2016;6:38946.
[36] Jin DY, Chae HZ, Rhee SG, Jeang KT. Regulatory role for a novel human thioreoxin peroxidase in NF-B activation. J Biol Chem 1997;272:30952–61.
[37] Rhee SG, Kang SW, Jeong W, Chang TS, Wang KS, Woo HA. Intracellular messenger function of hydrogen peroxide and its regulation by peroxiredoxins. Curr Opin Cell Biol 2005;17:183–9.
[38] Koussounadis A, Langdon SP, Um IH, Harrison DH, Smith VA. Relationship between differentially expressed mRNA and mRNA-protein correlations in a xenograft model system. Sci Rep 2015;5:10775.
[39] Ivanina AV, Sokolova IM, Sukhotin AA. Oxidative stress and expression of chaperones in aging mollusks. Comp Biochem Physiol B Biochem Mol Biol 2008;150:53–61.
[40] Rea IM, McNerlan S, Pckley AG. Serum heat shock protein and anti-heat shock protein antibody levels in aging. Exp Gerontol 2001;36:341–52.
[41] Lee YH, Lee JC, Moon HJ, Jung Je, Sharma M, Park BH, Yi HK, Jhee EC. Differential effect of oxidative stress on the apoptosis of early and late passage human diploid fibroblasts: implication of heat shock protein 60. Cell Biochem Funct 2008;26:502–8.
[42] Chen L, Na R, Ran Q. Enhanced defense against mitochondrial hydrogen peroxide attenuates age-associated cognition decline. Neurobiol Aging 2014;35:2552–61.
[43] Olahova M, Veal EA. A peroxiredoxin, PRDX-2, is required for insulin secretion and insulin/IIS-dependent regulation of stress resistance and longevity. Aging Cell 2015;14:558–68.
[44] Kayashima Y, Yamakawa-Kobayashi K. Involvement of Prx3, a Drosophila ortholog of the thiol-dependent peroxidase PRDX3, in age-dependent oxidative stress resistance. Biomed Res 2012;33:319–22.